



Synthesis and characterization of iron sulfide powders and its application for sorption of europium radionuclides

Karam Fatwhi Allan, Shiraz Labib*, Mohamed Holeil

Nuclear Chemistry Department, Hot Laboratories Center, Egyptian Atomic Energy Authority, P.O. Box 13759, Cairo, Egypt, Tel. +20 1114473191; email: karamallan@yahoo.com (K.F. Allan), Tel. +20 1005292059; email: dr_sh_labib@yahoo.com (S. Labib), Tel. +20 1117186420; email: [holiel_m@yahoo.com](mailto:holieil_m@yahoo.com) (M. Holeil)

Received 6 July 2015; Accepted 13 September 2015

ABSTRACT

In this research, cubic iron sulfide powder was prepared for the sorption of $(^{152} + ^{154})\text{Eu(III)}$ from the aqueous solutions. The prepared sorbents were characterized by: X-ray diffraction analysis, differential thermal analysis, thermogravimetric analysis, Fourier transform infrared, scanning electron microscope and energy dispersive X-ray analysis. The sorption was performed as a function of pH, contact time, temperature, and metal ion concentrations in the batch experiments. The results demonstrated that the sorption was well described by the Langmuir adsorption isotherm with the maximum adsorption capacity of $(0.0203 \text{ mmol g}^{-1})$. The kinetic data indicated that the sorption fitted well with the pseudo-second-order kinetic model. The thermodynamic parameters implied that the sorption process was spontaneous and endothermic in nature.

Keywords: Cubic iron sulfide; Characterization; Sorption; $(^{152} + ^{154})\text{Eu(III)}$

1. Introduction

Low- and intermediate-level radioactive wastes were produced during the research activities of the radiochemical laboratories, research reactors, radioisotope, and metallurgical laboratories, activation analysis units, nuclear medicine divisions in hospitals, universities, and research institutes as well as industrial activities [1,2]. Europium belongs to the lanthanide group of elements and only the trivalent oxidation state is stable in water. The ionic radii are almost the same for all the trivalent lanthanides and Am(III) which result in a chemically similar behavior. Europium is often chosen for the sorption investigations because it is easy to work with it in the laboratory [3–5]. The tracer most commonly used ^{152}Eu is a

β/γ -emitter, whereas Am is an α -emitter. The solubility of europium hydroxide is strongly dependent on pH with a solubility product, $\log K_{so} = 17.6$, for the amorphous phase. Because the ionic radius of Eu(III) is fairly large, 0.95 \AA , hydrolysis in solutions do not become appreciable until pH 6 is reached [6,7]. Europium poses an external as well as internal health hazard. The strong gamma radiation associated with ^{152}Eu and ^{154}Eu makes the external exposure to these two isotopes is of high concern [8]. While in the body, europium poses a health hazard from both the beta particles and gamma rays, and the main health concern is associated with the increased likelihood of inducing cancer in the liver and bone [8]. The most stable oxidation state for the elements in the lanthanide series, including europium, is the trivalent [8].

*Corresponding author.

Removal of lanthanides from the waste solutions could be achieved by several processes such as chemical reduction [9], solvent extraction [10], ion exchange [11], or sorption [12,13]. Among them sorption technique seemed to be a promising approach that offered a number of benefits such as reducing solvent usage, disposal costs, and extraction time.

Iron sulfides are an interesting class of materials with many different forms which include: pyrite (cubic- FeS_2), marcasite (calcium chloride structure- FeS_2), troilite (FeS), mackinawite (Fe_{1+x}S), pyrrhotite (Fe_{1-x}S , Fe_7S_8), smythite (hexagonal- Fe_3S_4), and greigite (cubic spinel- Fe_3S_4) [14]. While the synthesis of iron oxide materials is well documented, the preparation of iron sulfide materials has remained unexplored until recently. Greigite (Fe_3S_4) is also of interest in modern material science [15]. Fe_3S_4 is a useful material which has excellent magnetic properties, electrochemical hydrogen storage properties, and so on. Importantly, Fe_3S_4 is an environment-friendly material and can be used as sorbents for the removal of heavy metals from the environment [16].

This omission may be due their complex crystal structures and physical properties [14]. Recently, Fe_3S_4 crystals have been obtained by several methods as hydrothermal route and single-source precursor approach [14]. Herein, we report the use of iron(III) complexes of dialkyldithiocarbamates as single-source precursors to synthesize iron sulfide powder. It is best of our knowledge that the use of iron sulfide powder for the sorption of europium is not studied before. The objective of this research is to conduct a study on the sorption phenomenon of europium radioactive isotopes from the aqueous solutions using the prepared iron sulfide. It was found that iron sulfide promoted high-removal capability for hazardous radionuclides from liquid radioactive waste. This material can be successively applied for the treatment of low-level liquid radioactive waste containing $(^{152} + ^{154})\text{Eu(III)}$ and hence the storage as well as disposal process will be facilitated.

2. Experimental

2.1. Chemicals and reagents

All the chemicals were of analytical grade and used as received without further purification: ferric nitrate ($\text{Fe}(\text{NO}_3)_3 \cdot 9\text{H}_2\text{O}$) [99% Merck, Germany], sodium diethyldithiocarbamate ($(\text{C}_2\text{H}_5)_2\text{NCSSNa} \cdot 3\text{H}_2\text{O}$) [97% BDH Chemicals, UK], europium oxide (Eu_2O_3) [99% Alfa Aesar], and deionized water from the Millipore water purification system (18.2 M Ω).

2.2. Radioactive isotopes

For preliminary radiochemical investigations, radioactive $(^{152} + ^{154})\text{Eu(III)}$ was produced through the irradiation of europium oxide at the Egyptian second research reactor, ETRR-2. Accurate amounts of europium oxide samples (about 10 mg) were wrapped in thin aluminum foils that were previously cleaned with acetone and finally placed in thick aluminum irradiation capsules. They were transferred to an aluminum irradiation box of length of 670 mm then irradiated in ETRR-2 core adjacent with thermal neutron flux of $10^{14} \text{ n cm}^{-2} \text{ s}^{-1}$ for about 4 h.

2.3. Synthesis of materials

The experiment was carried out by adjusting the temperature to (30–40)°C, once 1 mol of sodium diethyldithiocarbamate, as complexing agent, was added to 1 mol of ferric nitrate solution a precipitate was formed. The formed precipitate was filtered off by centrifugation then washed with distilled water and absolute ethanol. The prepared powder was dried at 100°C (FS0) for 48 h then calcined at 300°C (FS3), 400°C (FS4), and 500°C (FS5) for 3 h. The sketch of iron sulfide material complexed within diethyldithiocarbamate is shown in Fig. 1.

It was known that diethyldithiocarbamate derivatives were S- and N-containing ligands which displayed a rich and varied coordination chemistry with a wide range of transition and main group metal complexes [17]. Diethyldithiocarbamate complexes constituted one of the most promising species to provide single-source materials for bulk metal sulfides [17].

2.4. Characterization

The prepared powders were characterized using X-ray diffraction (Shimadzu 6000, Japan). The used X-ray tube is a copper tube operating at 40 kV and 30 mA, and the used wavelength $k_{\alpha 1}$ is 1.54056 Å. The scan was performed over the range 2θ (4–90)°. The identification of the present crystalline phases was done using the Joint Committee on Powder Diffraction Standards (JCPDS) database card numbers. Thermolysis of the synthesized materials were studied using differential thermal analysis (DTA) and thermogravimetric procedure (TGA) using a Shimadzu simultaneous DTA/TGA-50 analyzer (Shimadzu, Japan). Spectra of the prepared hybrid materials were measured using Fourier transform infrared (FTIR) (Nicolet is10 spectrometer, Meslo, USA). Scanning electron microscopy (SEM) and energy dispersive X-ray analysis (EDX) of the synthetic adsorbent materials were

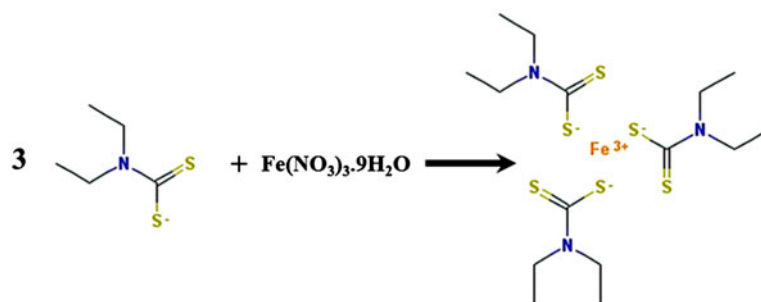


Fig. 1. Preparation sketch of iron sulfide exchanger.

examined using JEOL analytical scanning electron microscope (JSM-6510 LA, Japan). The scan was performed at high vacuum mode using an accelerating voltage of 25 kV, a working distance of 12 mm, and magnification 5,000 \times and 2,000 \times . Gamma radioactivity level throughout this work was measured using a gamma counter containing a NaI-Tl scintillation counter of the type Nucleus-Model 500 and scalar rate amplifier model 2010.

2.5. Batch distribution studies

The synthesized materials were undertaken using the batch contact method. Typically for the preliminary pH and contact time studies, the initial pH of the solutions was adjusted by adding either hydrochloric acid or liquid ammonia solutions for adjusting the medium at constant pH; a HANNA 30X model pH meter was used. The pH of the solution was adjusted with buffer at 4 except for as laid down elsewhere. At this point, the amount sorbed and contact time profiles were conducted in order to explore the equilibrium point. Once the equilibrium time was known, the different pH measurements were carried out for each ion. For this purpose, 10 ml of aqueous solutions of Eu(III) traced by $^{152} + ^{154}\text{Eu}$ with initial concentration $10^{-4} \text{ mol l}^{-1}$ was shaken with 0.03 g of the synthesized material at 298 K. Thereafter, 1 ml was withdrawn for radiometric assay using the NaI-Tl scintillation detector connected to the nucleus counting system for $^{152} + ^{154}\text{Eu}$.

The uptake percentage, % U , on the solid could be calculated from Eq. (1):

$$U \% = \frac{C_0 - C}{C_0} \times 100 \quad (1)$$

where C_0 and C are the concentration of sorbed ions (mol l^{-1}) before and after equilibrium.

The distribution coefficient, k_d (ml g^{-1}), could be also calculated from Eq. (2):

$$k_d = \frac{C_0 - C}{C} \times \frac{V}{W} \quad (2)$$

where V is the volume of solution (l) and W is the dry weight of the material (g).

2.6. Sorption isotherms

Sorption isotherm experiments were unambiguously conducted batchwise; the equilibrium was attained by shaking 0.03 g of the dried material in 10 ml of the aqueous solutions containing $10^{-4} \text{ mol l}^{-1}$ Eu(III) traced by $^{152} + ^{154}\text{Eu}$ which was shaken at 160 rpm for a predetermined time period in an incubator at a controlled temperature. The solution was filtered and the metal ion concentrations were measured. Initial and equilibrium concentrations of the metal ions in the aqueous phase were determined radiometrically. The pH of the solution was buffered only at 4, except for as laid down elsewhere as outlined above. Since the sorption experiments were temperature controlled, temperature-influenced experiments were carried out between 298 and 333 K at optimum pH values for $^{152} + ^{154}\text{Eu}$ (III) on the sorbent. The experiments were repeated three times in each case, the amount of metal ion sorbed by employing the same general protocol and analysis procedure as the batch contact experiments, except that the given metal concentration was increased, while the prepared iron sulfide powder was the only exchanger under test; the amount of metal ions sorbed per gram of the material q_e (mmol g^{-1}) was obtained by Eq. (3) as follows:

$$q_e = \frac{C_0 - C}{W} \times V \quad (3)$$

2.7. Kinetic experiments

The rate of sorption for a specific cation was followed with time by adding 10 ml of aqueous solution

having a concentration of 10^{-4} mol l $^{-1}$ Eu(III) traced by $^{152} + ^{154}\text{Eu}$ to 0.03 g of the dried material in penicillin bottle. Several bottles were prepared and kept in a thermostat shaker bath at 298 K for various periods of time. The sorption of the ions on the prepared material was followed with time until the equilibrium was attained for each ion in different batches.

2.8. Temperature effects

The temperature effect was taken into account between 298 and 333 K at optimum pH values for $(^{152} + ^{154})\text{Eu(III)}$ on the sorbent. The experiments were repeated three times in each case. The amount of the sorbed metal ions was calculated from 10 ml of aqueous solutions having a concentration of 10^{-4} mol l $^{-1}$ Eu(III) traced by $^{152} + ^{154}\text{Eu}$ added to 0.03 g of the dried material of at equilibrium.

3. Results and discussion

3.1. Characterization

3.1.1. X-ray diffraction analysis (XRD)

The phase, crystallinity, and purity of the prepared powders were determined by means of XRD technique. Fig. 2(a)–(d) shows the X-ray diffraction pattern of the as-prepared and thermally treated iron sulfide powders at 300, 400, and 500 °C for 3 h, respectively. The diffraction pattern of the as-prepared powder was characterized by the presence of cubic- Fe_3S_4 (JCPDS file No. 89-1998) as a major phase and very small peaks of cubic- FeS_2 (JCPDS 42-1340), Fig. 2(a). On the other hand, the increase in temperature to 300 °C showed an increase in the peak intensity of Fe_3S_4 and a slight decrease in the peak intensity of FeS_2 , Fig. 2(b). Otherwise with the increase in temperature to 400 °C, a marked decrease in the reflection peaks of Fe_3S_4 and FeS_2 was observed and a new phase of cubic- Fe_3O_4 (JCPDS 65-3107) was developed, as shown in Fig. 2(c). Further increase in the temperature to 500 °C showed the disappearance of both Fe_3S_4 and FeS_2 phases and the development of rhombohedral $\alpha\text{-Fe}_2\text{O}_3$ (JCPDS 33-0664), Fig. 2(d).

As concluded, iron sulfide powder was mainly present in the as-prepared powder (FS0) as well as the powder thermally treated at 300 °C (FS3); while the powders thermally treated at 400 °C (FS4) and 500 °C (FS5) were characterized by the presence of iron oxide phases. Another important note was that FS3 showed better crystalline behavior than FS0 due to the increase in the peak intensity of its Fe_3S_4 phase and the decrease in the peak intensity of its FeS_2 phase, as shown in Fig. 2(b).

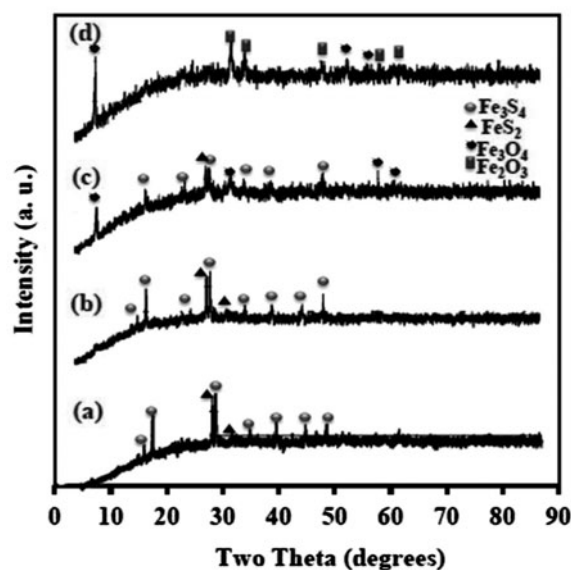


Fig. 2. XRD patterns of the as-prepared and thermally treated powders (a) FS0, (b) FS3, (c) FS4, and (d) FS5.

3.1.2. Differential thermal analysis–thermogravimetric analysis (DTA–TGA)

Thermal properties of the prepared powders were investigated in detail by designating the temperature in the range of 25–1,000 °C using DTA–TGA analysis and the corresponding curves are shown in Fig. 3. In general, the thermochemistry of metal diethyldithiocarbamates has been widely studied in the past years, but little was known about their decomposition kinetics [17]. TGA curve shows two weight losses at $T < 300$ °C. The first weight loss could be assigned to the evaporation and elimination of the bonded water, residual organic solvents. This result was correlated to the two small endothermic peaks of the DTA curve at $T < 100$ °C [18,19]. Whereas the second weight loss could be estimated to the decomposition of the sodium diethyldithiocarbamate iron complexes [20]. So, the TGA curve revealed that the formed complexes either volatilized leaving a negligible amount of residue or decomposed to yield iron sulfide as previously reported [17]. The third distinct weight loss ~6% at $T \geq 400$ °C was due to the development of Fe_3O_4 as indicated from the sharp endothermic peak given in the DTA curve, Fig. 3. This result was confirmed by the XRD data given in Fig. 2(c) that revealed the development of Fe_3O_4 at 400 °C. The as-prepared Fe_3S_4 sample could be converted into Fe_3O_4 sample at the calcination temperature exceeding 400 °C in air. Another weight loss ~18.67% at $T > 600$ °C was observed that was attributed to the complete

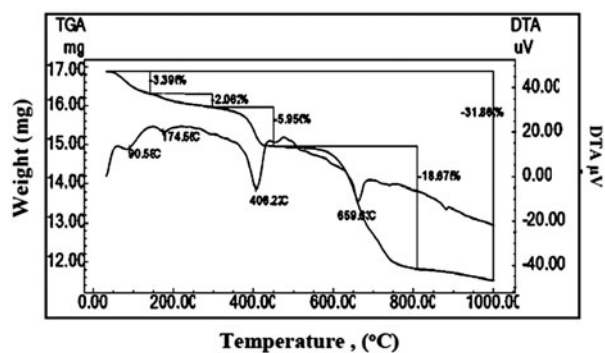


Fig. 3. DTA-TGA analysis of the prepared powder in air.

formation of α - Fe_2O_3 and was confirmed by a small endothermic peak at $T \sim 660^\circ\text{C}$.

3.1.3. Fourier transform infrared spectroscopy (FTIR) analysis

Fig. 4(a)–(e) shows the FTIR spectrum of the as-prepared powder, thermally treated powders, and FS3/Eu(III). The observed broad band at $\sim 3,400\text{ cm}^{-1}$ and small band at $\sim 1,627\text{ cm}^{-1}$ in all the prepared powders corresponded to both the stretching and bending vibrations mode H–O–H of physically adsorbed water from the atmosphere, respectively, Fig. 4(a)–(e) [21,22]. Very small band at $2,300\text{ cm}^{-1}$ was due to the adsorbed or atmospheric CO_2 , Fig. 4(a)–(e) [23]. FS0 showed many peaks due to the contribution of the diethyldithiocarbamate compound including the presence of both bending C–H ($1,100$ – $1,550\text{ cm}^{-1}$) and stretching C–H ($2,998$ – $2,954\text{ cm}^{-1}$) vibrations [24]. The characteristic peaks at $1,625$, $1,024$, $1,200$, and $1,012\text{ cm}^{-1}$ were attributed to thiocarbonyl (C=S)-stretching vibrations and indicated a symmetrical bidentate binding of the dithiocarbamate moiety [24], the peaks at ($1,350$ – $1,250\text{ cm}^{-1}$) were attributed to the stretching vibrations of (C–N), Fig. 4(a). A new band of medium to strong intensity observed in the region 420 – 405 cm^{-1} may be assigned to $\nu(\text{M–S})$ stretching mode, Fig. 4(a) [25]. The peak at 628 and 668 cm^{-1} corresponded to (S–S) stretching vibration, Fig. 4(a) [26,27]. In general, the presence of similar bands at $1,000$ – $1,200\text{ cm}^{-1}$ in FS0, FS3, and FS4 may be assigned to pyrite [28] and greigite formation as complexed within diethyldithiocarbamate derivative [28]. These results were also confirmed by the presence of bands of low intensity in the regions of $2,046$ and $1,900\text{ cm}^{-1}$ that were attributed to Fe–S vibration, Fig. 4(a) and (b) [29]. All these peaks have not been recorded in the spectrum of FS5 indicating the disappearance of FeS_2 and Fe_3S_4 phases for the powders

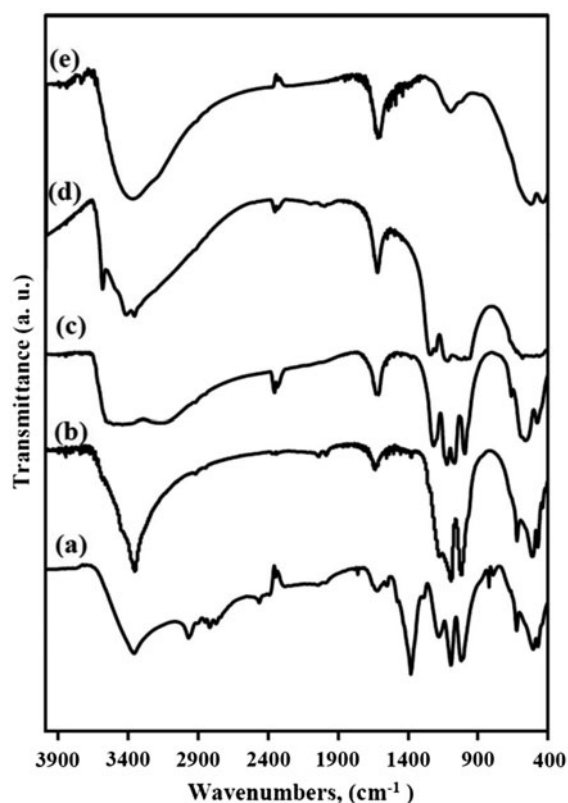


Fig. 4. FTIR spectra of the as-prepared (a) FS0, thermally treated powders (b) FS3, (c) FS4, (d) FS5, and (e) FS3/Eu(III).

thermally treated at 500°C and confirming the XRD and DTA-TGA results. Peaks observed at 565 and 580 cm^{-1} in FS4 and FS5 samples were assigned to Fe–O peaks [30] and corresponded to the formation of Fe_3O_4 and Fe_2O_3 , respectively, Fig. 4(c) and (d). FTIR spectra of the sample FS3 loaded with Eu(III) showed the disappearance of the peaks corresponding to the diethyldithiocarbamate complexed within Fe(III) confirming that the sorption of Eu(III) was taking place onto the active sites of Fe(III) complexed within diethyldithiocarbamate, Fig. 4(e).

3.1.4. Scanning electron microscopy (SEM)

SEM measurements were carried out in order to understand the morphology and the shape of synthesized powders. SEM micrographs of both the as-prepared and thermally treated powders are shown in Fig. 5(a)–(d). There were no noticeable morphological changes between the as-prepared powder (FS0) shown in Fig. 5(a) and the powder thermally treated at 300°C (FS3) shown in Fig. 5(b), where the powders consisted of uniform particles having a cubic shape. Subsequent changes were observed in FS4 where the cubic

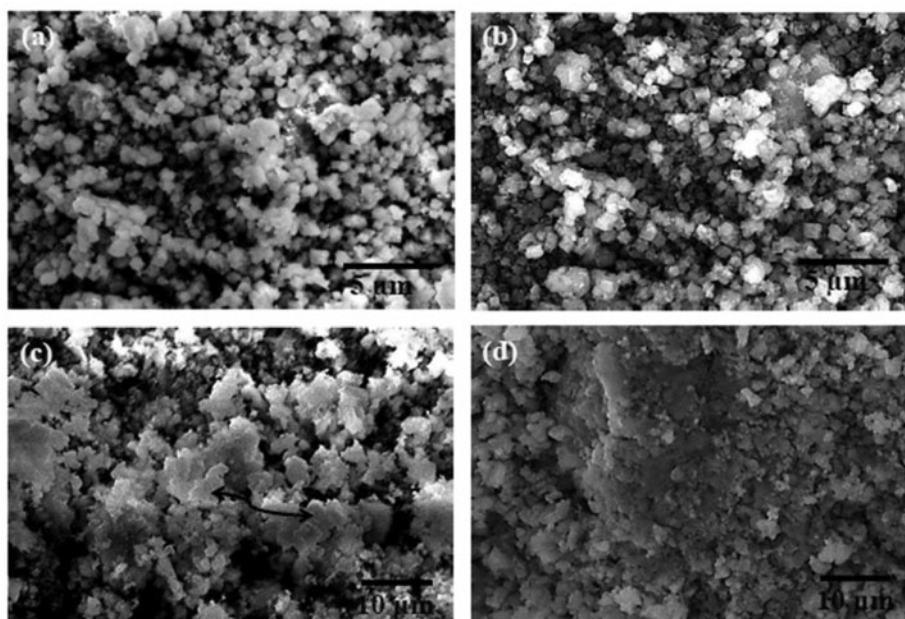


Fig. 5. SEM of the as-prepared and thermally treated powders (a) FS0, (b) FS3, (c) FS4, and (d) FS5.

particles transformed to rhomboid particles collapsed over some, as marked by black arrows shown in Fig. 5(c), and distributed over newly formed small particles of Fe_3O_4 . FS5 consisted of a more compacted distribution of Fe_3O_4 and Fe_2O_3 particles, Fig. 5(d).

3.1.5. Energy dispersive X-ray analysis

Fig. 6(a) and (b) shows the EDX spectra of both FS0 and FS3, respectively. EDX spectra of FS0 shows intense peaks for the elements Fe, S, C, O, and Na. The presence of Fe and S indicated the formation of iron sulfide complexed with carbamate derivative, Fig. 6(a). Also the presence of C and O indicated the presence of various carbon- and oxygen-containing functional groups at the surface. On the other hand, the EDX spectra of FS3 given in Fig. 6(b) showed a decrease in the peaks of C and O due to the thermal effect as outlined above in the DTA-TGA data. The increase in the peak intensity of Fe and S meaning that there was an improvement in the crystallization of Fe_3S_4 . So, the EDX results confirmed the results obtained in both the XRD and FTIR results. We have observed the absence of N element peak in both spectra and the only reason that we could propose was the interference of both the peaks of N (k_α : 0.392) with that of O (k_α : 0.525), especially the small difference between the k_α values [31]. In this case, the identification of nitrogen and quantification of its content,

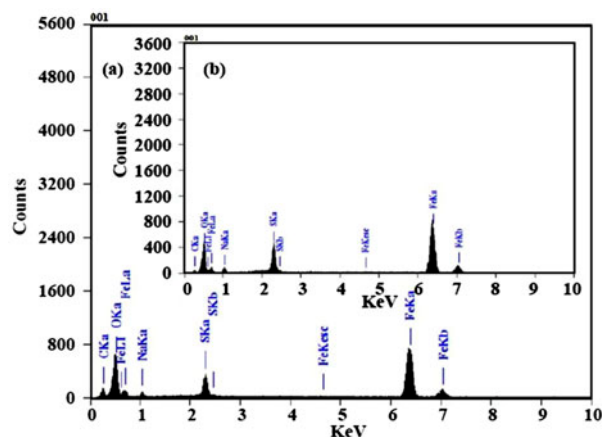


Fig. 6. EDX spectra of (a) the as-prepared powder “FS0” and (b) the powder thermally treated at 300°C for 3 h “FS3”.

which was very low, is often tricky and may appear a little bit confusing [31].

According to this study, FS0 and FS3 showed many similarities from the point of view of XRD, SEM, and FTIR, but we have selected FS3 to be the material used as a sorbent for $^{152} + ^{154}\text{Eu(III)}$ because it showed better crystalline behavior as given in XRD investigations and higher percent of Fe and S elements as given in EDX results.

3.2. Batch sorption studies

3.2.1. Effect of pH value

Sorption phenomenon of metal ions by sorbents is pH dependent; this may be assigned to the discrepancies in either their possible complexation reactions or physisorption processes at the sorption surface. The initial pH of the solution is an important parameter which controls the sorption process. It affects the surface of the sorbent and the chemistry of metal ion in solution. The effect of pH on sorption of $(^{152} + ^{154})\text{Eu}$ (III) on FS3 at initial concentration of $\text{Eu(III)} 1.0 \times 10^{-4}$ (mol L^{-1}) was studied in the pH range 2–5 to avoid any complications from the precipitation of Eu(III) at higher pH in the aqueous solution [32]. The hydrolysis of Eu(III) begins at pH as low as 6 and various species can be formed [32]. Fig. 7 shows the pH dependence of $(^{152} + ^{154})\text{Eu(III)}$ sorption on FS3 at an initial concentration of $\text{Eu(III)} \times 10^{-4} \text{ mol l}^{-1}$ as outlined before. As shown in Fig. 7, the solution pH was the key factor that affects the sorption of Eu(III) on FS3 powder. The sorption of $(^{152} + ^{154})\text{Eu(III)}$ increased slowly at pH 0.5–2 and sorbed abruptly at pH 2–3.5. Then, the sorption remained constant up to pH 3.5 for Eu(III) as shown in Fig. 7. This may be attributed to the competition between the higher concentration of H ions present in the reaction mixture and the Eu(III) for the sorption sites and as such no sorption occurred below pH 0.5. Above this pH, the concentration of H ion decreased, whereas the concentration of Eu(III) remained constant. The sorption of Eu(III) in this range could be explained as an H– Eu(III) exchange reaction. After this pH range, the hydroxide species could be formed and form hydroxocomplexes [33,34]. This behavior could be attributed to the change of the speciation products

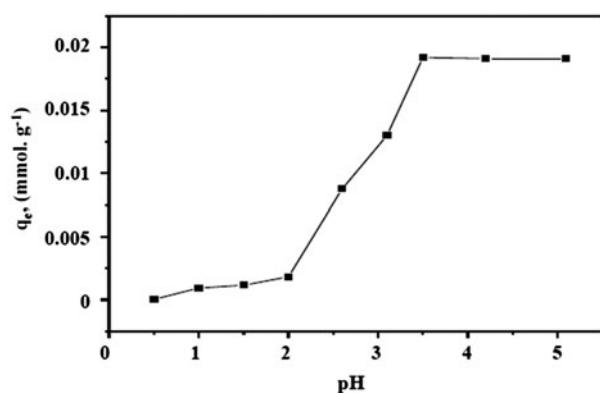


Fig. 7. Effect of pH on the sorption capacity of $(^{152} + ^{154})\text{Eu(III)}$ on FS3 sorbent: C_o (10^{-4}), sorbent dose (0.05 g), shaking time (60 min), and temp. (298 K).

and the involved sorption mechanism at the solid–liquid interface with pH variation [35].

3.2.2. Effect of sample weight

The relationship between the sample weight and the amount of $(^{152} + ^{154})\text{Eu(III)}$ sorbed on FS3 sample is shown in Fig. 8. It was observed that the amount sorbed increased with increasing the weight of FS3 sample up to 0.09 g, while at higher amounts q_e values remained constant. Close inspection to the data clarified that the amount sorbed attained the value of $0.0128 \text{ mmol g}^{-1}$ with 5 mg of sample weight while it attained $0.01572 \text{ mmol g}^{-1}$ with 10 mg of sample. Therefore, the increase in q_e value from 0.0192 to $0.0211 \text{ mmol g}^{-1}$ was not consisted with the increase in sample weight from 5 to 10 mg. So, it was supposed to consider 5 mg as a sample weight in the rest of experiments.

3.2.3. Effect of ionic strength

The effect of ionic strength, adjusted with NaCl salt, on $(^{152} + ^{154})\text{Eu(III)}$ sorption on FS3 was presented in Fig. 9. The data clarified that q_e of $(^{152} + ^{154})\text{Eu(III)}$ decreased with the increasing ionic strength molarity. This was because the movement of $(^{152} + ^{154})\text{Eu(III)}$ from the bulk solution toward the sorbent surface was retarded by the presence of an increased concentration of Na(I) ions that formed a positive layer on the surface of the applied sorbent. Also, Na(I) could compete with $(^{152} + ^{154})\text{Eu(III)}$ for the available active sites on the sorbent surface. It is wise to note that the high ionic charge of $(^{152} + ^{154})\text{Eu(III)}$ compared with that of

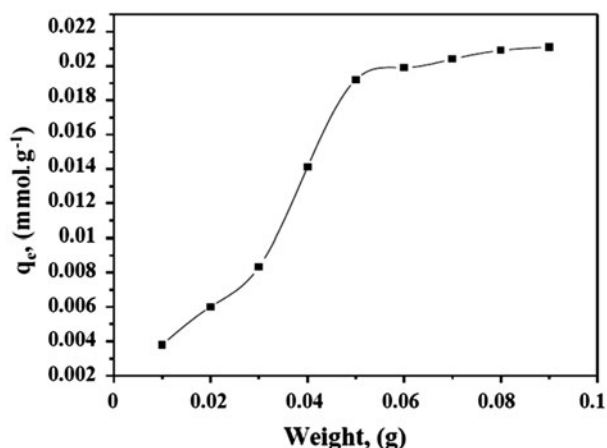


Fig. 8. Variation of $(^{152} + ^{154})\text{Eu(III)}$ sorbed on FS3 sorbent with sample weight.

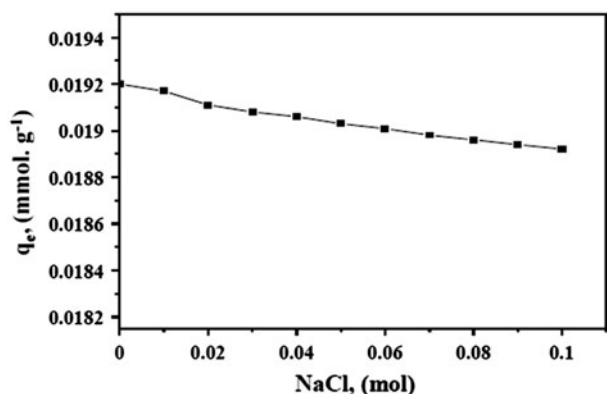


Fig. 9. Variation of $(^{152} + ^{154})\text{Eu(III)}$ sorbed on FS3 sorbent with NaCl as background electrolyte.

Na(I) depressed the competitive action of Na(I). Therefore, the overall q_e values were slightly decreased by the presence of an increased concentration of NaCl as a background electrolyte.

3.3. Sorption isotherm

At equilibrium, the amount of solute being sorbed onto the sorbent is equal to the amount of solute being desorbed and the solution concentration remains constant (C_e). The sorption isotherm described the removal of $(^{152} + ^{154})\text{Eu(III)}$ from the aqueous solution on FS3 at 298 K is shown in Fig. 10. There were many isotherms that could be used for modeling the sorption process in heterogeneous systems. Of these models, Langmuir, Freundlich, and Dubinin–Radushkevich (D–R) isotherms were considered in this study and their parameters were obtained from the logarithmic form of the isotherm equations.

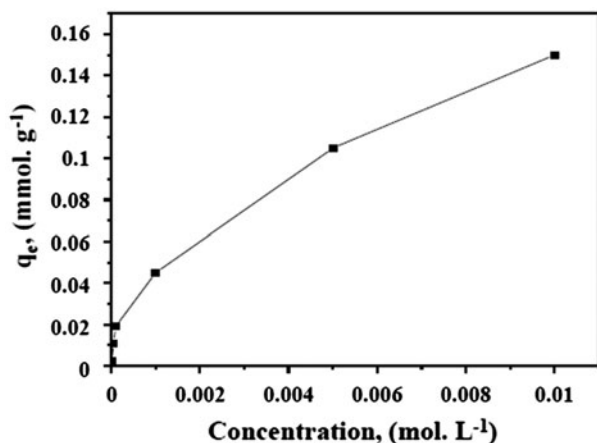


Fig. 10. Sorption isotherms of $(^{152} + ^{154})\text{Eu(III)}$ on FS3 at 298 K.

3.3.1. Langmuir isotherm

The linearized form of Langmuir isotherm equation could be written in Eq. (4) as follows [36]:

$$\frac{1}{q_e} = \frac{1}{q_m} + \frac{1}{bq_m C_e} \quad (4)$$

where q_e is the amount of the solute sorbed per unit weight of the sorbent (mmol g^{-1}) as outlined before, C_e is the equilibrium concentration of the solute in the equilibrium solution (mol l^{-1}), q_m is the monolayer sorption capacity (mmol g^{-1}), and b is a constant related to the free energy of sorption ($b \propto e^{-\Delta G/RT}$). As shown in Fig. 11(a), the plot of $1/q_e$ vs. $1/C_e$ should give a straight line and the Langmuir constants could be calculated. The essential features of the Langmuir isotherm could be expressed in terms of equilibrium

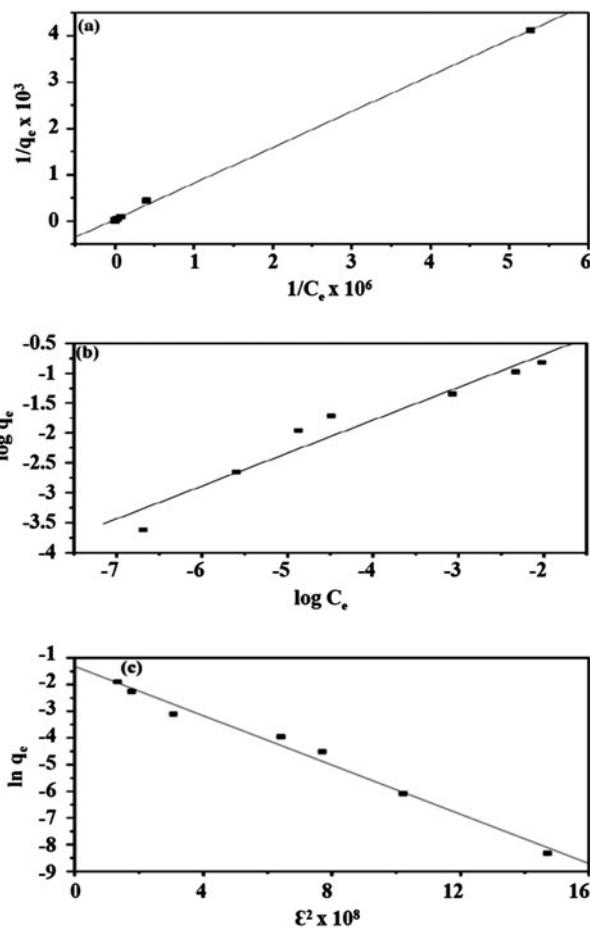


Fig. 11. (a) Langmuir model for the sorption of $(^{152} + ^{154})\text{Eu(III)}$ on FS3 sorbent, (b) Freundlich model for the sorption of $(^{152} + ^{154})\text{Eu(III)}$ on FS3 sorbent, and (c) D–R isotherms of $(^{152} + ^{154})\text{Eu(III)}$ on FS3 sorbent.

Table 1
Langmuir, Freundlich, and D–R isotherm constants

FS ₃ sorbent	Langmuir parameters	q_m (mmol g ⁻¹) 0.0262685	b (L mmol ⁻¹) 49,261.083	R_L 0.203	R^2 0.9996
	Freundlich parameters	K_F (mmol g ⁻¹) 2.5678		n 1.82	R^2 0.9685
	D–R parameters	q_m (mmol g ⁻¹) 0.267	k (mol ² kJ ⁻²) 4.62E-9	ε (kJ mol ⁻¹) 10.416	R^2 0.9928

parameter, R_L , which was used to predict if the sorption system was “favorable” or “unfavorable” [37,38].

$$R_L = \frac{1}{1 + bC_0} \quad (5)$$

where C_0 is the initial metal concentration. The value of R_L indicated the shape of an isotherm to be either unfavorable ($R_L > 1$), linear ($R_L = 1$), favorable ($0 < R_L < 1$), or irreversible ($R_L = 0$). These values were less than unity indicating that the sorption was favorable and the used sorbent was optimum for the sorption of ^(152 + 154)Eu(III) from the aqueous solutions.

3.3.2. Freundlich isotherm

Freundlich isotherm models the multilayer sorption that postulated the heterogeneity of surfaces; its linearized form was given by the following equation [39]:

$$\log q_e = \log K_F + \frac{1}{n} \log C_e \quad (6)$$

where K_F is the Freundlich constant (mmol g⁻¹) which indicated the sorption capacity and represented the strength of the adsorptive bond and n is the heterogeneity factor. The plot of $\log q_e$ vs. $\log C_e$ may give a straight line as shown in Fig. 11(b), K_F and n values could be calculated from the intercept and slope of this straight line, respectively.

3.3.3. D–R isotherms

In D–R model, the sorption on a single type of uniform pores was adopted. In this manner, the D–R isotherm was an analog of the Langmuir type in a more general postulation that it did not assume a homogeneous surface or constant sorption potential [40].

The D–R isotherm was given as follows:

$$q_e = q_m \exp(-k\varepsilon^2) \quad (7)$$

The linearized form of this equation was given by:

$$\ln q_e = \ln q_m - k\varepsilon^2 \quad (8)$$

where ε (Polan’s potential) is $[RT \ln(1 + (1/C_e))]$, k is a constant related to the sorption energy (mmol² kJ⁻²). The values of q_m and k were calculated from the intercept and slope of the D–R plot, respectively, and presented in Table 1. The mean free energy of sorption (ε) could be calculated from the corresponding k values using the equation:

$$\varepsilon = \frac{1}{\sqrt{-2k}} \quad (9)$$

The magnitude of ε , based on D–R model as shown in Fig. 11(c), was considered as a useful mean for estimating the type of sorption process.

It was evident from these data that the sorption fitted well to the Langmuir isotherm model than that of the Freundlich and D–R models, as indicated from the numerical values of the correlation coefficients (R^2). A reasonable explanation for this result was: Eu(III) traced by ^(152 + 154)Eu(III) in the aqueous solution was sorbed on the surface of FS3 and formed a monolayer through the coordination of ^(152 + 154)Eu(III) with the lone pair of electrons present on the sulfur atom in diethyldithiocarbamate complexed within Fe(III), (Fig. 1). Therefore, the Langmuir model fitted the experimental data better than the Freundlich model and D–R models. The maximum sorption capacity of the sorbent, calculated from the Langmuir isotherm equation, defined the total capacity of the sorbent for rare earth ions. It was found that the sorption capacity of ^(152 + 154)Eu(III) using

FS3 ($0.0203 \text{ mmol g}^{-1}$) was consistent with the results obtained from the pH effect on the sorption. In addition, the magnitude of ε was considered as a useful mean for estimating the type of the sorption process as outlined above. If this value was between 8 and 16 kJ mol^{-1} , the sorption process could be explained by ion exchange [41]. In this study, ε value was estimated to be $10.416 \text{ kJ mol}^{-1}$, as shown in Table 1. Consequently, the sorption of $(^{152} + ^{154})\text{Eu(III)}$ on FS3 could be explained by ion exchange process.

3.4. Sorption kinetic studies

Kinetic studies were undertaken to show the mechanistic aspects of the process and obtain the thermodynamic parameters. In order to interpret the experimental data, it was necessary to identify the best-fit model that represented the sorption process. The kinetics of the sorption was important since it controlled the efficiency of the process. The sorption process was generally fast at the beginning and then slowed down as the equilibrium was approached. Fig. 12 shows the variation of the amounts of $(^{152} + ^{154})\text{Eu(III)}$ sorbed on FS3 at different time intervals, for a fixed initial ion concentration of $10^{-4} \text{ mol l}^{-1}$ and sorption temperature at 298 K. The amount removed of $(^{152} + ^{154})\text{Eu(III)}$ from the solution increased with time, and about 84% of equilibrium was reached within the first 10 min. It was well recognized that the characteristic of the sorbent surface was a critical factor that affected the sorption rate parameters and that the diffusion resistance played an important role in the overall transport of the ion [42,43]. The high capacity of FS3 toward $(^{152} + ^{154})\text{Eu(III)}$ sorption could be attributed to the presence of the lone pair of electrons on the sulfur atom in diethyldithiocarbamate complexed within Fe(III), (Fig. 1) as outlined before. The rate constant of $(^{152} + ^{154})\text{Eu(III)}$ removal from the

solution by FS3 was determined using pseudo-first-order, pseudo-second-order rate, and intraparticle diffusion models.

3.4.1. Lagergren pseudo-first-order model

Lagergren pseudo-first-order expression was written as follows [44]:

$$\ln(q_e - q_t) = \ln q_e - (k_1)t \quad (10)$$

where q_e and q_t (mmol g^{-1}) are the amount of $(^{152} + ^{154})\text{Eu(III)}$ sorbed on FS3 at equilibrium and time t , respectively. k_1 is the pseudo-first-order rate constant (min^{-1}). Pseudo-first-order kinetic for the sorption of $(^{152} + ^{154})\text{Eu(III)}$ on FS3 was studied to determine the first-order rate constant (k_1) and the theoretical equilibrium sorption capacities (q_e), respectively. The calculated values of k_1 and q_e with the values of the linear correlation coefficients (R^2) were presented in Table 2. The theoretically calculated equilibrium sorption capacity should be in accordance with the experimental sorption capacity values. As could be seen from Table 2, both the linear correlation coefficients (R^2) of the plot and the q_e (calculated) values differ with q_e (experimental) for the studied sorption process. So, it could be suggested that the sorption of $(^{152} + ^{154})\text{Eu(III)}$ on FS3 was not a first-order reaction.

3.4.2. Pseudo-second-order model

In order to find a more reliable description of the kinetics, pseudo-second-order kinetic equation was applied. The kinetic data were tested by the pseudo-second-order expression as follows [45]:

$$\frac{t}{q_t} = \frac{1}{k_2 q_e^2} + \left(\frac{1}{q_e}\right)t \quad (11)$$

where k_2 is the rate constant of pseudo-second-order equation ($\text{g mg}^{-1} \text{ min}^{-1}$). Thus, by plotting t/q_t against t the value of k_2 , q_e , and the product $k_2 q_e^2$ (which represents the rate of the initial sorption) could be determined graphically from the slope and the intercept of the revealed plot. The kinetics plot of t/q_t vs. t for $(^{152} + ^{154})\text{Eu(III)}$ removal on FS3 is represented in Fig. 13. The equilibrium metal sorption capacity (q_e), the values of the rate constant (k_2), and the correlation coefficients (R^2) were calculated and presented in Table 2. The plot was linear and the corresponding correlation coefficients (R^2) suggested a strong relationship between the calculated mathematical

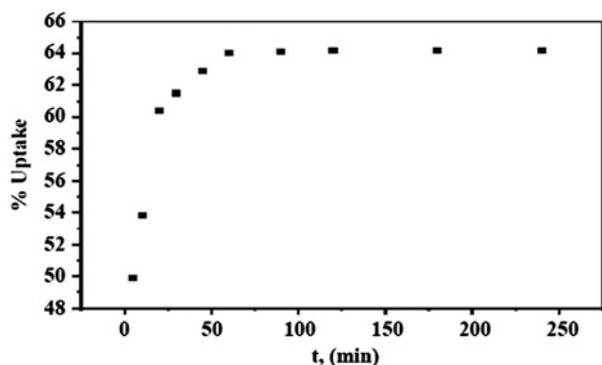


Fig. 12. Variation of the amounts of $(^{152} + ^{154})\text{Eu(III)}$ sorbed on FS3 sorbent at different time intervals.

Table 2
Pseudo-first-order, pseudo-second-order, and intraparticle diffusion rate models

FS ₃ sorbent	Experimental result		$q_{e(\text{exp.})}$ (mmol g ⁻¹) 0.0203	
	Pseudo-first-order rate constants	k_{ads} (min ⁻¹) 0.05545	$q_{e(\text{theo.})}$ (mmol g ⁻¹) 0.0055	R^2 0.9996
	Pseudo-second-order rate constants	k_2 (mmol g ⁻¹ m ⁻¹) 22.272	$q_{e(\text{theo.})}$ (mmol g ⁻¹) 0.0197	R^2 0.9998
	Intraparticle diffusion constants	k_{id} (mmol g ⁻¹ min ^{-1/2}) 0.0137	C (mmol g ⁻¹) 0007581	R^2 0.982

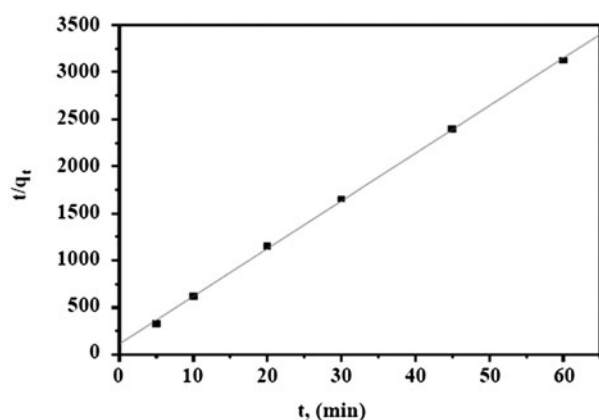


Fig. 13. Pseudo-second-order kinetic for the sorption of ^(152 + 154)Eu(III) on FS3 sorbent.

parameters and also explained that the process of the sorption of each ion followed the pseudo-second-order kinetics. Also from the data, it was observed that the correlation coefficient (R^2) had an extremely high value (>0.99) and closer to unity for the pseudo-second-order kinetic model than for the pseudo-first-order kinetic model. When comparing the obtained value for the sorption capacity (q_e) with the calculated value of q_e , using pseudo-second-order kinetic model, we found a good agreement with the experimental data clarifying the matching of the experimental data to the pseudo-second-order kinetics. The results explained that the pseudo-second-order kinetic was predominant and that the rate constant of the sorption appeared to be controlled by an ion exchange process through sharing or exchange of electrons between iron sulfide exchange surface and the exchanging of ^(152 + 154)Eu(III) [45].

3.4.3. Intraparticle diffusion model

The solute transport from a solution phase to the surface of iron sulfide occurred in several steps:

external diffusion, surface diffusion, pore diffusion, and sorption on the pore surface, or a combination of more than one step. The overall sorption process may be controlled either by one or more of these steps. In rapidly stirred batch sorption, the diffusive mass transfer could be related to an apparent diffusion coefficient, which will fit the experimental sorption rate data. In general, the sorption process is diffusion controlled if its rate is dependent upon the rate at which components diffuse toward one another. The possibility of intraparticle diffusion was explored using the intraparticle diffusion model given by Weber–Morris and represented by the equation [46]:

$$q_t = k_{\text{id}}t^{0.5} + C \quad (12)$$

where k_{id} is the intraparticle diffusion rate constant ($\text{mg g}^{-1} \text{min}^{-0.5}$) and C is a constant (mg g^{-1}) that gives an idea about the thickness of the boundary layer, i.e. the larger the value of C , the greater the boundary layer effect. If Weber–Morris plot of q_t vs. $t^{0.5}$ gave a straight line, then the sorption process was controlled by intraparticle diffusion only. However, if the data exhibited multilinear plots, then two or more steps influenced the sorption process. Weber and Morris plots of ^(152 + 154)Eu(III) sorbed per unit mass of adsorbent vs. $t^{0.5}$ for FS3 are given in Fig. 14. The slope of these plots was defined as a rate parameter that was characteristic to the rate of sorption in the region where intraparticle diffusion was the controlling rate. The graphs revealed that the data points were related by two straight lines: the first portion depicting macropore diffusion and the second one representing micropore diffusion. The extrapolation of the linear portions of the plots to the y -axis gave the intercept, which provided a measure of the boundary layer thickness. The deviation of the straight line from the origin may be due to the difference in the rate of mass transfer in the initial and final stages of sorption. Further, such

deviation of straight line from the origin indicated that the pore diffusion was not the sole rate-controlling step. The sorption data for q_e vs. $t^{0.5}$ for the initial period showed a curvature that was usually attributed to the boundary layer diffusion effects or external mass transfer effects. The values of model parameters of the intraparticle diffusion rate constant (k_{id}) and the correlation coefficient (R^2) are shown in Table 2. It was likely supposed that a large number of $(^{152} + ^{154})\text{Eu(III)}$ diffused into the pores before being sorbed. Significantly, the plot did not have a zero intercept as proposed by Eq. (12) indicating that the intraparticle diffusion might not be the controlling factor in determining the kinetics of the process. As shown in Fig. 14, the plots of q_t vs. $t^{0.5}$ did not fit with the straight lines passing through the origin as required by Eq. (12) indicating the non-applicability of this model and the intraparticle diffusion was not the rate-controlling step during the sorption process of $(^{152} + ^{154})\text{Eu(III)}$ on FS3 sorbent. When the transport of the solute from the liquid phase to the solid phase boundary played the most significant role in the sorption, the liquid film diffusion model may be applied using Boyd kinetic expression as shown in Eq. (13) [47]:

$$F = 1 - \frac{6}{\pi^2} \exp(-B_t) \quad (13)$$

where F is the fraction of the sorbate sorbed at different times t ($F = q_t/q_e$) and B_t is a mathematical function of F . The rearrangement of Eq. (13) gives:

$$B_t = -0.4977 - \ln \left[1 - \frac{q_t}{q_e} \right] \quad (14)$$

The calculated B_t values for $(^{152} + ^{154})\text{Eu(III)}$ sorption on FS3 were plotted against t as shown in Fig. 15. The

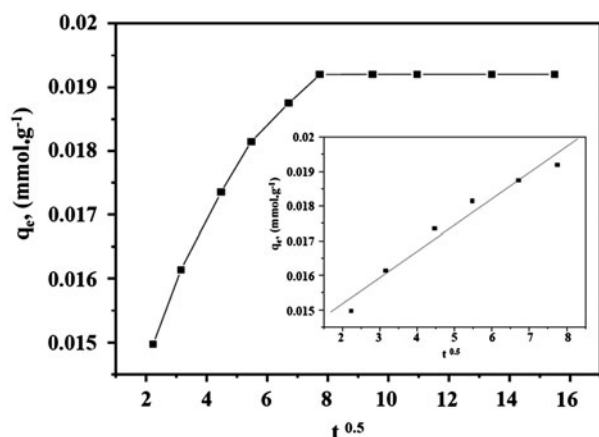


Fig. 14. Morris–Weber plots for modeling of $(^{152} + ^{154})\text{Eu(III)}$ sorbed on FS3 sorbent.

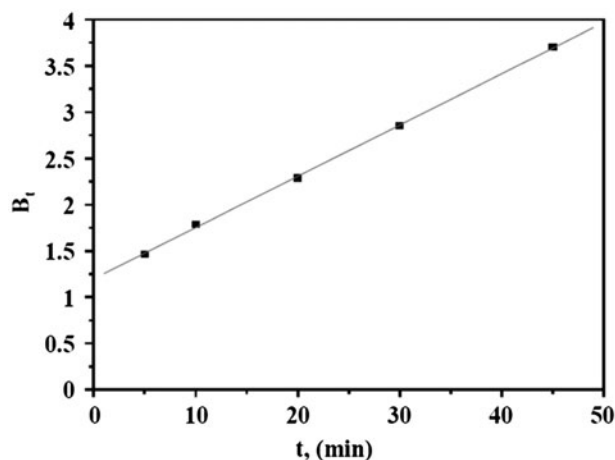


Fig. 15. Correlation between B_t and t for the sorption of $(^{152} + ^{154})\text{Eu(III)}$ on FS3 sorbent.

linearity of the plot will provide useful information for distinguishing between the external transport- and intraparticle transport-controlled rates of sorption [48]. In general, if the plot of B_t vs. t gave a straight line passing through the origin, then the sorption was governed by a particle diffusion mechanism. Otherwise, it was governed by film diffusion. From Fig. 15, the plot was not only deviated from the origin, but also it had a very poor linear correlation coefficient, R^2 is 0.98541, implying that the external mass transport (film diffusion) is the rate-controlling step throughout the sorption process of $(^{152} + ^{154})\text{Eu(III)}$ on FS3 sorbent. Several investigations reported that sorption of heavy metals onto various adsorbents was film diffusion controlled [49,50].

3.5. Effect of reaction temperature

The entire study was performed at five temperatures: 298, 303, 313, 323, and 333 K to evaluate the thermodynamic properties after attaining equilibrium at 60 min for $(^{152} + ^{154})\text{Eu(III)}$. A 0.033-g mass of FS3 material and 10 ml of $10^{-4} \text{ mol l}^{-1}$ from each ion were equilibrated at their natural equilibrium pH of 3.5 $(^{152} + ^{154})\text{Eu(III)}$. The plot of q_e against the temperature is shown in Fig. 16. The experimental fitting of the data revealed that the linear relationship between the amount sorbed and temperature has been obtained. This could be explained by the reversible behavior of the sorption process at the solid–liquid interface. The thermodynamic parameters of the sorption reactions were calculated using Van't Hoff's equation, from the slope of the linear relationship of plotting $\log K_c$ against $1/T$ as shown in the inset of Fig. 16.

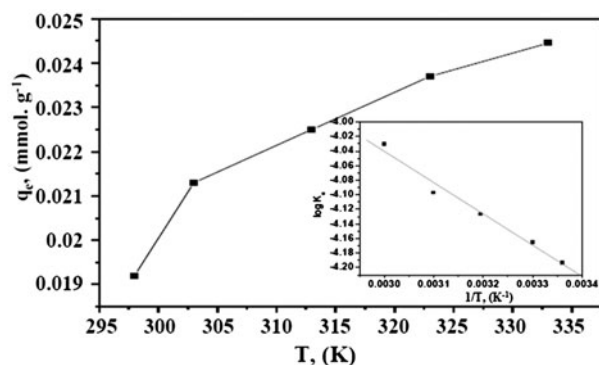


Fig. 16. Effect of temperature on the sorption modeling of $(^{152} + ^{154})\text{Eu(III)}$ sorbed on FS3 sorbent. The inset shows Van't Hoff plot for $(^{152} + ^{154})\text{Eu(III)}$ sorbed on FS3 sorbent.

Table 3

Thermodynamic parameters for sorption of $(^{152} + ^{154})\text{Eu(III)}$ sorbed on FS3 powder

	ΔH° (kJ mol $^{-1}$)	ΔS° (J mol $^{-1}$ K $^{-1}$)	T (K)	ΔG° (kJ mol $^{-1}$)
FS ₃ sorbent	8.22	52.7	298	-15.700
			303	-16.620
			313	-17.700
			323	-18.873
			333	-19.897

From this plot; the thermodynamic parameters were calculated using the following relations, Eqs. (15)–(18):

$$\Delta G = -2.303RT \log K_c \quad (15)$$

where K_c is the sorption equilibrium constant, R is the gas constant (8.314 J mol $^{-1}$ K $^{-1}$), and T is the absolute temperature (K). The sorption equilibrium constant (K_c) could be calculated from the relation given in Eq. (16):

$$K_c = \frac{F_e}{1 - F_e} \quad (16)$$

where F_e is the fraction attainment of the metal ion sorbed at equilibrium, which is defined as the ratio between the sorbed ion concentration at certain instant and the equilibrium concentration.

$$\log K_c = \frac{\Delta S}{2.303R} - \frac{\Delta H}{2.303RT} \quad (17)$$

$$\Delta S = \frac{\Delta H - \Delta G}{T} \quad (18)$$

where ΔH is the enthalpy change of the sorption process, ΔG is the free energy change, and ΔS is the entropy change. The thermodynamic parameters are summarized in Table 3.

The positive values of ΔH indicated the endothermic nature of the sorption process and its value 8.22, the prepared FS3 reflected an ion exchange and implied the possibility of strong bonding between $(^{152} + ^{154})\text{Eu(III)}$ and the sorbent surface [48]. The negative values of ΔG indicated a spontaneous nature and a high preference of $(^{152} + ^{154})\text{Eu(III)}$ sorption on the used material. The positive values of ΔS specified the increasing of randomness at the powder–aqueous medium interface during the sorption process [51].

4. Conclusion

Iron sulfide powders with homogeneous cubic shape were successfully prepared using a single-source precursor approach, where diethyldithiocarbamate was used as a complexing agent. Both the as-prepared powder (FS0) and thermally treated powder at 300°C (FS3) were considered as the source of iron sulfide material (Fe_3S_4) in this work because at higher temperatures (400 and 500°C), iron oxide phases (Fe_3O_4 and Fe_2O_3) were formed. FS0 and FS3 showed the formation of Fe_3S_4 as a major phase and FeS_2 as a minor phase, but FS3 showed better crystallinity behavior and was used as a sorbent for $(^{152} + ^{154})\text{Eu(III)}$. A detailed study for the sorption of $(^{152} + ^{154})\text{Eu(III)}$ on FS3 was given, where the prepared iron sulfide powder exhibited promising sorption for $(^{152} + ^{154})\text{Eu(III)}$ from the aqueous solution. The sorption equilibrium data were fitted with Langmuir, Freundlich, and Dubinin–Radushkevitch isotherm models. The results indicated that the isotherm data were successfully fitted Langmuir over the entire concentration range studied. Furthermore, the kinetics of the metal ions were experimentally studied and the obtained rate data were analyzed using simple Lagergren-first-order, pseudo-second-order, and intra-particle diffusion models. The results explained that the pseudo-second-order sorption mechanism was predominant and the overall rate constant of the sorption process appeared to be controlled by ion exchange process. The process was thermodynamically feasible as indicated by a negative free energy change and a positive entropy change which confirmed that the process was endothermic in nature. Finally, cubic iron sulfide as a green sorbent material could be successively applied for the treatment of radioactive liquid waste.

References

- [1] R.O. Abdel Rahman, A.A. Zaki, A.M. El-Kamash, Modeling the long-term leaching behavior of ^{137}Cs , ^{60}Co , and $^{152,154}\text{Eu}$ radionuclides from cement–clay matrices, *J. Hazard. Mater.* 145 (2007) 372–380.
- [2] M.I. El-Dessouky, M.R. El-Sourougy, H.F. Aly, Investigations on the treatment of low and medium level radioactive liquid wastes, *Isotopenpraxis* 26 (1990) 608–611.
- [3] B.K. Singh, R. Tomar, S. Kumar, A. Jain, B.S. Tomar, V.K. Manchanda, Sorption of ^{137}Cs , ^{133}Ba and ^{154}Eu by synthesized sodium aluminosilicate (Na-AS), *J. Hazard. Mater.* 178 (2010) 771–776.
- [4] B.K. Singh, A. Jain, S. Kumar, B.S. Tomar, R. Tomar, V. Manchanda, Role of magnetite and humic acid in radionuclide migration in the environment, *J. Contam. Hydrol.* 106 (2009) 144–149.
- [5] B.K. Singh, R. Tomar, S. Kumar, A.S. Kar, B.S. Tomar, S. Ramanathan, Role of the humic acid for sorption of radionuclides by synthesized titania, *Radiochim. Acta* 102 (2014) 255–261.
- [6] R.C. Weast, *Handbook of Chemistry and Physics*, 60th ed., CRC Press, Boca Raton, FL, 1980.
- [7] M.H. Bradbury, B. Baeyens, Sorption of Eu on Na- and Ca-montmorillonites: Experimental investigations and modelling with cation exchange and surface complexation, *Geochim. Cosmochim. Acta* 66 (2002) 2325–2334.
- [8] S.I. Moussa, Synthesis and characterization of magnetic nano-materials for removal of metal ions from aqueous solutions, Ph.D. Thesis, Faculty of Sciences, Ain Shams University, Cairo, Egypt, 2013.
- [9] C.A. Morais, V.S.T. Ciminelli, Recovery of europium by chemical reduction of a commercial solution of europium and gadolinium chlorides, *Hydrometallurgy* 60 (2001) 247–253.
- [10] A. Bhattacharyya, P.K. Mohapatra, T. Gadly, D.R. Raut, S.K. Ghosh, V.K. Manchanda, Liquid–liquid extraction and flat sheet supported liquid membrane studies on Am(III) and Eu(III) separation using 2,6-bis(5,6-dipropyl-1,2,4-triazin-3-yl)pyridine as the extractant, *J. Hazard. Mater.* 195 (2011) 238–244.
- [11] L. Jelinek, Y.Z. Wei, T. Arai, M. Kumagai, Study on separation of Eu(II) from trivalent rare earths via electro reduction and ion exchange, *J. Alloy Compd.* 451 (2008) 341–343.
- [12] P. Sharma, G. Singh, R. Tomar, Synthesis and characterization of an analogue of heulandite: Sorption applications for thorium(IV), europium(III), samarium(II) and iron(III) recovery from aqueous waste, *J. Colloid Interface Sci.* 332 (2009) 298–308.
- [13] D.L. Guerra, R.R. Viana, C. Airolidi, Use of raw and chemically modified hectorites as adsorbents for Th(IV), U(VI) and Eu(III) uptake from aqueous solutions, *Desalination* 260 (2010) 161–171.
- [14] M. Akhtar, J. Akhter, M.A. Malik, P. O'Brien, F. Tuna, J. Raftery, M. Helliwell, Deposition of iron sulfide nanocrystals from single source precursors, *J. Mater. Chem.* 21 (2011) 9737–9745.
- [15] G. Li, B. Zhang, F. Yu, A.A. Novakova, M.S. Krivenkov, T.Y. Kiseleva, L. Chang, J. Rao, A.O. Polyakov, G.R. Blake, R.A. de Groot, T.T.M. Palstra, High-Purity Fe_3S_4 greigite microcrystals for magnetic and electrochemical performance, *Chem. Mater.* 26 (2014) 5821–5829.
- [16] X. Wang, W. Cai, G. Wang, Z. Wu, H. Zhao, One-step fabrication of high performance micro/nanostructured $\text{Fe}_3\text{S}_4\text{-C}$ magnetic adsorbent with easy recovery and regeneration properties, *Cryst. Eng. Comm.* 15 (2013) 2956–2965.
- [17] T.K. Jana, D.P. Kumar, R. Pradhan, S. Dinda, P.N. Ghosh, C. Simonnet, J. Marrot, I. Imaz, A. Wattiaux, L. Fournès, J.-P. Sutter, F. Sécheresse, R. Bhattacharyya, Synthesis and structure of iron(III) and iron(II) complexes in S4P2 environment created by diethyldithiocarbamate and 1,2-bis(diphenylphosphino)ethane chelation: Investigation of the electronic structure of the complexes by Mössbauer and magnetic studies, *Inorg. Chim. Acta* 362 (2009) 3583–3594.
- [18] M. Li, M. Xu, H. Liang, X. Li, T. Xu, Preparation and Dielectric Properties of Mn-Doped $\text{Ba}_{0.6}\text{Sr}_{0.4}\text{TiO}_3\text{-MgTiO}_3$ composite ceramics, *Acta Phys. Chim. Sin.* 24 (2008) 1405–1410.
- [19] Sh. Anas, P. Mukundan, A.M. Sanoj, V.R. Mangalaraja, S. Ananthakumar, Synthesis of ZnO based nanopowders via a non-hydrolytic sol gel technique and their densification behaviour and varistor properties, *Process. Appl. Ceram.* 4 (2010) 7–14.
- [20] D.C. Onwudiwe, P.A. Ajibade, Thermal studies of Zn(II), Cd(II) and Hg(II) complexes of some N-alkyl-N-phenyl-dithiocarbamates, *Int. J. Mol. Sci.* 13 (2012) 9502–9513.
- [21] S.W. Boland, S.C. Pillai, W.D. Yang, S.M. Haile, Preparation of (Pb, Ba)TiO₃ powders and highly oriented thin films by a sol–gel process, *J. Mater. Res.* 19 (2004) 1492–1498.
- [22] I. Bibi, B. Singh, E. Silvester, Akaganéite ($\beta\text{-FeOOH}$) precipitation in inland acid sulfate soils of south-western New South Wales (NSW), Australia, *Geochim. Cosmochim. Acta* 75 (2011) 6429–6438.
- [23] S. Maensiri, C. Masingboon, B. Boonchom, S. Seraphin, A simple route to synthesize nickel ferrite (NiFe_2O_4) nanoparticles using egg white, *Scripta Mater.* 56 (2007) 797–800.
- [24] A. Bossi, M.J. Whitcombe, Y. Uludag, S. Fowler, I. Chianella, S. Subrahmanyam, I. Sanchez, S.A. Piletsky, Synthesis of controlled polymeric cross-linked coatings via iniferter polymerisation in the presence of tetraethyl thiuram disulphide chain terminator, *Biosens. Bioelectron.* 25 (2010) 21499–22155.
- [25] M. Sharma, A. Sharma, R. Sachar, Preparation and characterization of the adducts of bis(N,N-diethyldithiocarbamato)oxovanadium(IV) and copper(II) with n-propylamine and isopropylamine, *Chem. Sci. Trans.* 2 (2013) 367–374.
- [26] N. Kandasamy, S. Saravanan, D.R. Nayak, Structural, optical and thermal studies on zinc sulfide nanorods and manganese sulfide nanoparticles, *IJACSA* 1 (2014) 25–30.
- [27] V. Krylova, Spectroscopic and diffraction studies of chemical deposition of copper sulfide films on polyamide surface using potassium pentathionate, *Mater. Sci. Poland* 25 (2007) 933–945.
- [28] R.K. Rath, S. Subramanian, T. Pradeep, Surface chemical studies on pyrite in the presence of polysaccharide-based flotation depressants, *J. Colloid Interface Sci.* 229 (2000) 82–91.

- [29] M.R.M. Chaves, K.T. Valsaraj, R.D. DeLaune, R.P. Gambrell, P.M. Buchler, Sediment Transport, first ed., Cratia, InTech, 2011, pp. 313–334.
- [30] N. Salamun, H.X. Ni, S. Triwahyono, A. Abdul Jalil, A.H. Karim, Synthesis and characterization of Fe₃O₄ nanoparticles by electrodeposition and reduction methods, *J. Fundam. Sci.* 7 (2011) 89–92.
- [31] M. Rabiller-Baudry, F. Gouttefangeas, J.L. Lannic, P. Rabiller, Méndez-Vilas A (Eds.), Handbook on Current Microscopy Contributions to Advances in Science and Technology, Formatex, Madrid, 2012.
- [32] E. Bentouhami, G.M. Bouet, J. Meullemestre, F. Vierling, M.A. Khan, Physicochemical study of the hydrolysis of rare-earth elements(III) and thorium(IV), *C.R. Chim.* 7 (2004) 537–545.
- [33] C. Boukhalifa, Sulfate removal from aqueous solutions by hydrous iron oxide in the presence of heavy metals and competitive anions: Macroscopic and spectroscopic analyses, *Desalination* 250 (2010) 428–432.
- [34] H.A. Omar, H. Moloukhia, Use of activated carbon in removal of some radioisotopes from their waste solutions, *J. Hazard. Mater.* 157 (2008) 242–246.
- [35] S.I. Moussa, R.R. Sheha, E.A. Saad, N.A. Tadros, Synthesis and characterization of magnetic nano-material for removal of Eu³⁺ ions from aqueous solutions, *J. Radioanal. Nucl. Chem.* 295 (2013) 929–935.
- [36] I. Langmuir, The adsorption of gases on plane surfaces of glass, mica and platinum, *J. Am. Chem. Soc.* 40 (1918) 1361–1403.
- [37] G. Bayramoglu, A. Senel, M.Y. Arica, Effect of spacer-arm and Cu(II) ions on performance of l-histidine immobilized on poly(GMA/MMA) beads as an affinity ligand for separation and purification of IgG, *Sep. Purif. Technol.* 50 (2006) 229–239.
- [38] G. Bayramoglu, S. Bektas, M.Y. Arica, Biosorption of heavy metal ions on immobilized white-rot fungus *Trametes versicolor*, *J. Hazard. Mater.* 101 (2003) 285–300.
- [39] M.D. Mashitah, Z. Zulfadhly, S. Bhatta, Binding mechanism of heavy metals biosorption by *Pycnoporus Sanguineus*, *Artif. Cells, Blood Substitutes, Immobilization Biotechnol.* 27 (1999) 441–445.
- [40] W. Rieman, H. Walton, Ion Exchange in Analytical: Chemistry International Series of Monographs in Analytical Chemistry, Pergamon Press, Oxford, 1970.
- [41] I. Mobasherpour, E. Salahi, M. Pazouki, Removal of nickel(II) from aqueous solutions by using nano-crystalline calcium hydroxyapatite, *J. Saudi Chem. Soc.* 15 (2011) 105–112.
- [42] A.A. Zaki, T. El-Zakla, M. Abed El Geleel, Modeling kinetics and thermodynamics of Cs⁺ and Eu³⁺ removal from waste solutions using modified cellulose acetate membranes, *J. Membr. Sci.* 401–402 (2012) 1–12.
- [43] A.M. El-kamash, A.A. Zaki, M. Abdel El Geleel, Modeling batch kinetics and thermodynamics of zinc and cadmium ions removal from waste solutions using synthetic zeolite A, *J. Hazard. Mater.* 127 (2005) 211–220.
- [44] S. Lagergren, About the theory of so-called adsorption of soluble substances, *K. Sven. Vetensk. Akad. Handl.* 24 (1898) 1–39.
- [45] F.A. Shehata, M.F. Attallah, E.H. Borai, M.A. Hilal, M.M. Abo-Aly, Sorption reaction mechanism of some hazardous radionuclides from mixed waste by impregnated crown ether onto polymeric resin, *Appl. Radiat. Isot.* 68 (2010) 239–249.
- [46] W.J. Weber, J.C. Morris, Kinetics of adsorption on carbon from solution, *J. Sanit. Eng. Div. Am. Soc. Civ. Eng.* 89 (1963) 31–59.
- [47] G.E. Boyd, A.W. Adamson, L.S. Myers, The exchange adsorption of ions from aqueous solutions by organic zeolites. II. Kinetics 1, *J. Am. Chem. Soc.* 69 (1947) 2836–2848.
- [48] C.-K. Lee, S.-S. Liu, L.-C. Juang, C.-C. Wang, K.-S. Lin, M.-D. Lyu, Application of MCM-41 for dyes removal from wastewater, *J. Hazard. Mater.* 147 (2007) 997–1005.
- [49] X.-J. Hu, J.-S. Wang, Y.-G. Liu, X. Li, G.-M. Zeng, Z.-L. Bao, X.-X. Zeng, A.-W. Chen, F. Long, Adsorption of chromium(VI) by ethylenediamine-modified cross-linked magnetic chitosan resin: Isotherms, kinetics and thermodynamics, *J. Hazard. Mater.* 185 (2011) 306–314.
- [50] M. Mahmoud, G.E. Sharaf El-deen, M.A. Soliman, Surfactant-impregnated activated carbon for enhanced adsorptive removal of Ce(IV) radionuclides from aqueous solutions, *Ann. Nucl. Energy* 72 (2014) 134–144.
- [51] K.F. Allan, M. Holiel, W.A. Sanad, Gamma radiation induced preparation of organic–inorganic composite material for sorption of cesium and zinc, *Radiochemistry* 56 (2014) 267–274.